Surface Pressure Drag for Hydrostatic Two-Layer Flow over Axisymmetric Mountains

MARTIN LEUTBECHER*

Institut für Physik der Atmosphäre, Deutsches Zentrum für Luft- und Raumfahrt, Oberpfaffenhofen, Germany

(Manuscript received 19 March 1999, in final form 5 July 2000)

ABSTRACT

The effect of partial reflections on surface pressure drag is investigated for hydrostatic gravity waves in two-layer flow with piecewise constant buoyancy frequency. The variation of normalized surface pressure drag with interface height is analyzed for axisymmetric mountains. The results are compared with the familiar solution for infinitely long ridges. The drag for the two-layer flow is normalized with the drag of one-layer flow. An analytical expression for the normalized drag of axisymmetric mountains is derived from linear theory of steady flow. Additionally, two-layer flow over finite-height axisymmetric mountains is simulated numerically for flow with higher stability in the upper layer. The temporal evolution of the surface pressure drag is examined in a series of experiments with different interface and mountain heights. The focus is on the linear regime and the nonlinear regime of nonbreaking gravity waves.

The entire spectrum of gravity waves can be in resonance in hydrostatic flow over infinitely long ridges. This cannot occur in 3D flow over isolated mountains due to the dispersion of gravity waves. In consequence, the oscillation of the normalized drag with interface height is smaller for axisymmetric mountains than for infinitely long ridges. However, even for a reflection coefficient as low as ⅓ the drag of an axisymmetric mountain can be amplified by 50% and reduced by 40%.

The nonlinear drag becomes steady in the numerical experiments in which no wave breaking occurs. The steady-state nonlinear drag agrees quite well with the prediction of linear theory if the linear drag is computed for a slightly lowered interface.

1. Introduction

Orographic gravity waves are known to redistribute momentum in the atmosphere. Their breaking results in a flow deceleration; this is a relevant momentum sink of the global circulation. The momentum is transferred from the atmosphere to the ground by the distribution of surface pressure on the slopes of the orography. The associated force, the surface pressure drag, is therefore a key quantity.

Much progress has been made in understanding stratified flow over orography by analyzing the linearized equations of motion (Smith 1979, 1989). Since the early work by Queney (1948) it is known that gravity waves induced by flow over a ridge result in an asymmetric distribution of surface pressure with high pressure upstream and low pressure downstream of the ridge crest. The sensitivity of the gravity wave response to the vertical structure of the atmosphere, in particular its stratification, has been studied by several authors for two-dimensional flow over ridges. These results will be discussed below. Furthermore, the surface pressure drag has been calculated analytically for certain idealized hydrostatic three-dimensional flows. For flow with constant mean wind and buoyancy frequency, Phillips (1984) derives expressions for the drag of a class of bell-shaped mountains with elliptical contours. Grubišić and Smolarkiewicz (1997) calculate the drag of a bell-shaped axisymmetric mountain in hydrostatic flow with constant buoyancy frequency and constant vertical shear—including the negative shear case, which has a critical level.

Atmospheric profiles often exhibit considerable changes of buoyancy frequency over vertical scales of less than a kilometer. Such a distinct change of atmospheric stability occurring in a shallow layer is regularly present at the thermal tropopause. At such inhomogeneities upward propagating gravity waves are partially reflected (Queney 1947). The reflections can reduce or enhance the drag compared to the value for a nonreflective atmosphere with a similar but smoother profile

* Current affiliation: European Centre for Medium-Range Weather Forecasts.

Corresponding author address: Martin Leutbecher, European Centre for Medium-Range Weather Forecasts, Shinfield Park, Reading, RG2 9AX, United Kingdom.
E-mail: M.Leutbecher@ecmwf.int

of buoyancy frequency. The reflectivity decreases with increasing depth of the layer in which the change of stability occurs (Blumen 1985). Multilayer atmospheres with constant buoyancy frequency in each layer have been considered as an idealization.

Scorer (1949) explained lee waves in terms of orographic gravity waves trapped in a tropospheric layer by total reflection. The reflection and transmission of gravity waves at an interface of two layers with different Scorer parameters are analogous to the behavior of electromagnetic waves at the interface of media with different refractive indices. Assuming a horizontal interface and linearized equations of motion for steady flow, the ratio of the amplitude of the reflected wave to the amplitude of the incident wave, the reflection coefficient, is $R = (m_1 - m_2)/(m_1 + m_2)$, where m_1 and m_2 are the vertical wavenumbers in the two layers (Zierep 1956; Eliassen and Palm 1960). Subscript 1 refers to the layer of the incident wave. Total reflection occurs if the wave is external to layer 2, that is, m_2 is imaginary. Only waves in the nonhydrostatic regime can be totally reflected for statically stable background flow. Lee waves require total or almost total reflection and resonance. Resonance occurs if the contributions to vertical velocity from the reflected wave and the upward propagating wave interfere destructively at the surface. Total reflection and resonance then lead to free modes, which are nontrivial solutions satisfying $w|_{z=0} = 0$. The reflection is always partial, $|R| < 1$, in hydrostatic flow (Blumen 1985). Resonance by partial reflection amplifies the amplitude of orographic gravity waves. This mechanism was explored as an explanation for downslope wind storms. The dependence of the surface wind maximum on the vertical structure of the atmosphere has been investigated by Klemp and Lilly (1975) for multilayer flow and by Blumen and Hartsough (1985) for atmospheres with continuous profiles of wind speed and buoyancy frequency. Smith (1977) studied partial resonance in two-layer flow over sinusoidal orography taking into account finite-amplitude effects with a second-order correction to linear theory.

Previous studies examined the surface pressure drag for two-layer flow in two-dimensional settings, that is, flow over infinitely long ridges. Blumen (1965) discusses the drag of a random orography for steady linear nonhydrostatic flow. The nonhydrostatic dispersion results in a Fourier integral that requires numerical evaluation. Gill (1982) calculates the drag for sinusoidal orography analytically. It is useful to normalize the drag for two-layer flow. Let N_1 and N_2 denote the buoyancy frequencies of the lower and upper layer, respectively. Then, the normalized drag is defined as the ratio between the two-layer drag and the drag for one-layer flow with buoyancy frequency N_1. As the interface height changes, the normalized drag varies in the range N_1/N_2 to N_2/N_1. Maximum (minimum) drag occurs, when the interface height is a multiple of one-half vertical wavelength for the case with higher stability in the upper (lower) layer. Stationary gravity waves in two-dimensional hydrostatic flow are nondispersive. Therefore, the normalized drag is independent of the shape of the orography and equals Gill's expression for sinusoidal orography.

The variation of surface pressure drag with interface height has not been studied yet for three-dimensional two-layer flow over isolated mountains. Steady hydrostatic flow over infinitely long ridges is special as the vertical wavenumber of gravity waves is independent of the horizontal wavenumber. Therefore the entire wave spectrum is resonant at the same interface height. In contrast, in three-dimensional flow over isolated mountains resonance occurs at different interface heights for different parts of the wave spectrum, as the vertical wavenumber varies with the orientation of the horizontal wavenumber vector. This argument suggests that the drag of an isolated mountain in hydrostatic two-layer flow will be less sensitive to interface height than the drag of an infinitely long ridge.

Linear theory describes the flow in the limit of vanishing mountain height accurately. The drag can depart from the predictions of linear theory for flow over finite-amplitude mountains. For flows with constant wind U and buoyancy frequency N, the drag of bell-shaped ridges increases abruptly over the value predicted by linear theory, when the dimensionless mountain height $h_* = h_0N/U$ exceeds a critical value near 1 (Clark and Peltier 1977; Durran 1986). These high-drag states are associated with wave overturning aloft and strong surface winds on the lee slope. The drag is two to five times larger than the linear value (Durran and Klemp 1987; Bacmeister and Pierrehumbert 1988). Departures of the drag from the linear theory prediction can be associated as well with wave overturning at higher steepening levels (Bacmeister and Schoeberl 1989) or nonbreaking finite-amplitude gravity waves induced by asymmetric mountain profiles (Lilly and Klemp 1979). The transition to high drag is known to occur also in three-dimensional flow over isolated mountains (Miranda and James 1992; Ólafsson and Bougeault 1997).

Nonlinear effects appear in flow with a structured static stability profile at lower mountain heights than in the case with constant buoyancy frequency. The drag in two-dimensional two-layer flow over a ridge can exceed the value predicted by linear theory by a factor of 3 at a dimensionless mountain height of 0.3 in a case with higher stability in the lower layer as numerical simulations by Durran (1986) show. The early onset of nonlinearity in two-layer flow over a ridge was further investigated by Durran (1992) using a hydrostatic model based on Long's equation. For the case with higher stability in the upper layer, he calculated the drag as function of interface height for various mountain heights up to 0.5. The nonlinear drag varies in a range that is almost identical to the range predicted by linear theory. The nonlinear drag equals the linear drag computed for a

lower interface height. The shift of interface height is approximately 1.5 times the ridge height.

In the present study, the variation of drag with interface height is calculated analytically for two-layer flow over an isolated mountain. The derivation is based on the linearized Boussinesq equations for steady hydrostatic flow. In addition, the flow is assumed to be adiabatic and inviscid. An axisymmetric mountain is considered in order to permit an analytic solution. Furthermore, the drag of an isolated finite-amplitude mountain is studied. The nonlinear regime of nonbreaking gravity waves is investigated with a series of numerical simulations for flow with higher stability in the upper layer.

The outline of the paper is as follows. Section 2 recapitulates the required parts of linear theory for two-layer flows. The variation of drag with interface height for two-dimensional flow is presented in section 3. This variation is then compared with the results for three-dimensional flow over axisymmetric mountains in section 4. Some lengthy algebra is summarized in the appendix. The results of the finite-amplitude experiments are presented in section 5. Section 6 contains discussion and conclusions.

2. Linear steady two-layer flow

The analysis starts with the linearized equations of motion for steady hydrostatic Boussinesq flow. Planetary rotation is not included and the flow is assumed to be adiabatic and inviscid. We consider a two-layer flow with piecewise constant buoyancy frequency,

$$N(z) = \left(-\frac{g}{\rho_{00}}\frac{d\rho_0}{dz}\right)^{1/2} = \begin{cases} N_2, & z > H \\ N_1, & 0 < z < H, \end{cases}$$

as basic state, where $\rho_0(z)$ denotes the density profile, $\rho_{00} = \rho_0(0)$ the surface value, and H the height of the interface between the two layers. Furthermore the basic-state flow is assumed to be unsheared $\mathbf{u}(\mathbf{x}) = (u_0, 0, 0)$. Flow over orography is described by using the linearized lower boundary condition for vertical velocity $w|_{z=0} = u_0 \partial h/\partial x$, where h denotes terrain height and is a function of x or (x, y) depending on mountain geometry.

The linear problem is solved formally as in the case with constant buoyancy frequency (Smith 1980). Fourier transformation in the horizontal direction leads to the ordinary differential equation

$$N^2(k^2 + l^2)\hat{w} + u_0^2 k^2 \frac{d^2\hat{w}}{dz^2} = 0 \tag{1}$$

for vertical velocity w (or alternatively vertical displacement). Here the hat denotes Fourier transformation and k, l are the wavenumbers in the x and y directions. An analytic solution of (1) is readily obtained for piecewise constant buoyancy frequency. The solution is discussed in section 2a. The perturbations of horizontal velocity components, density, and pressure are obtained from $\hat{w}$ via the Fourier transformed linearized Boussinesq equations. For the pressure perturbation $\hat{p}$, the relation

$$\hat{p} = -i\rho_{00}u_0 \frac{k}{k^2 + l^2}\frac{d\hat{w}}{dz} \tag{2}$$

holds. The inverse Fourier transform yields the formal solution for the perturbations in physical space.

In the following the n-dimensional forward Fourier transform is defined by $\hat{\eta}(\mathbf{k}) = \int \eta(\mathbf{x}) \exp[-i\mathbf{k}\cdot\mathbf{x}]\, d^n x$, where $\mathbf{x} = (x_1, \ldots, x_n)$, $\mathbf{k} = (k_1, \ldots, k_n)$ are the spatial coordinate and wavenumber vector, and $\int d^n x$ denotes the n-dimensional volume integral. The inverse of this transform is given by the same definition except that the sign in the argument of the exponential is changed and the integral is normalized with $(2\pi)^{-n}$. A one-dimensional transformation is used for infinitely long ridges and a two-dimensional transformation for isolated mountains.

a. Partial reflection and resonance

In the spirit of linear theory the boundary conditions at the interface are linearized. The linearized kinematic and dynamic condition require the continuity of vertical velocity $\hat{w}$ and pressure pertubation $\hat{p}$ at $z = H$. From these boundary conditions the reflection coefficient is obtained as

$$R = -\frac{N_2 - N_1}{N_2 + N_1}, \tag{3}$$

and the transmission coefficient as $T = 1 + R$, where the incident wave is in layer 1.

The solution of (1) is composed of three plane waves:

$$\hat{w}(z) = \mu A_{1L} \times \begin{cases} (1 + R)\exp[+im_2 z + i(m_1 - m_2)H] & \text{if } z > H, \\ (\exp[+im_1 z] + R\exp[-im_1 z + i2m_1 H]) & \text{if } z \le H, \end{cases} \tag{4}$$

assuming upward energy propagation in the upper layer. In the lower layer, waves with upward and downward energy propagation are superimposed. In layer $i = 1, 2$ the vertical wavenumber m_i satisfies the dispersion relation

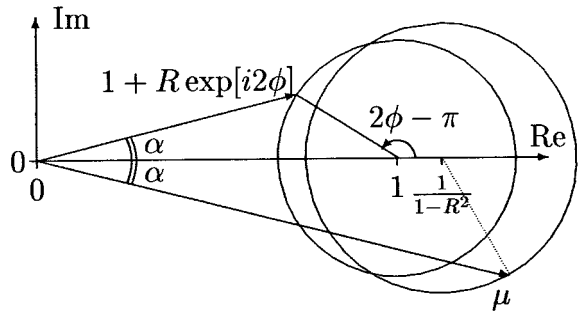

FIG. 1. Geometric interpretation of tuning factor $\mu = (1 + R \exp[i2\phi])^{-1}$ in the complex plane. The tuning factor is located on a circle of radius $|R|/(1 - R^2)$. The position on the circle is determined by the phase shift $\phi = m_1 H$ of the gravity wave across the lower layer. This drawing represents a reflection coefficient of $R = -\frac{1}{3}$.

$$m_i = \frac{N_i}{u_0}\frac{K}{k} = \frac{N_i}{u_0 \cos\psi}, \tag{5}$$

where K and ψ denote the magnitude and azimuth of the wavenumber vector (k, l), respectively. The choice of sign of the vertical wavenumber ascertains upward (downward) energy propagation for waves of the form $\exp[+imz](\exp[-imz])$.

The lower boundary condition $\hat{w}|_{z=0} = iku_0\hat{h}$ determines the amplitude μA_{1L}. For a one-layer atmosphere ($N_i = N$), the solution is $\hat{w}_{1L} = A_{1L} \exp[imz]$ with amplitude $A_{1L} = iku_0\hat{h}$. The amplitude is modified by the coefficient $\mu = (1 + R \exp[i2m_1H])^{-1}$ for a two-layer atmosphere. The locus of μ describes a circle in the complex plane as the interface height H is varied (Fig. 1). The magnitude of μ ranges from $(1 - R)^{-1}$ to $(1 + R)^{-1}$. Resonance, that is maximum $|\mu|$, occurs if the contributions to vertical velocity from the upward-propagating and downward-propagating waves interfere destructively at the surface. This happens if the interface height is an integer multiple of one-half vertical wavelength for the case of higher stability in the upper layer. In the other case ($N_2 < N_1$), the resonant interface heights are one-quarter vertical wavelength lower.

The Fourier amplitude of surface pressure is obtained from (2) and (4):

$$\hat{p}|_{z=0} = \rho_{00}u_0^2\frac{ik^2m_1}{k^2 + l^2}\gamma\hat{h} = \gamma\hat{p}_{1L}|_{z=0} \quad \text{with} \tag{6a}$$

$$\gamma = \frac{1 - R \exp(i2m_1H)}{1 + R \exp(i2m_1H)}. \tag{6b}$$

The amplitude for two-layer flow is proportional to $\hat{p}_{1L}|_{z=0}$, which denotes the pressure perturbation for one-layer flow with buoyancy frequency N_1. The factor γ expresses the influence of partial reflections on surface pressure. In the case of resonance, the contributions to pressure from the upward- and downward-propagating waves interfere constructively at the surface.

b. Surface pressure drag

Surface pressure drag refers to the force exerted on orography by the distribution of surface pressure. The drag in the x direction is given by the integral of $p|_{z=h}\partial h/\partial x$ over the area with nonzero gradient of terrain height h. It is common to calculate the drag to leading order in linear theory. Therefore, $p|_{z=h}$ is approximated by $p|_{z=0}$ to simplify the calculations.

The drag can be written as an integral in wavenumber space by using the Fourier representation of surface pressure and integrating partially. The drag of an isolated mountain is then given by

$$D = -\frac{1}{4\pi^2}\int_{-\infty}^{+\infty}\int_{-\infty}^{+\infty} ik\hat{h}^*\hat{p}|_{z=0}\, dk\, dl. \tag{7}$$

Complex conjugation is denoted by superscript ''*.'' Similarly, the drag per unit length D' of an infinitely long ridge is given by

$$D' = -\frac{1}{2\pi}\int_{-\infty}^{+\infty} ik\hat{h}^*\hat{p}|_{z=0}\, dk$$

$$= -\frac{1}{\pi}\mathrm{Re}\int_{0}^{+\infty} ik\hat{h}^*\hat{p}|_{z=0}\, dk, \tag{8}$$

where Re denotes the ''real part of.''

3. Drag of infinitely long ridges

Gravity waves are nondispersive in hydrostatic steady 2D flow. In each layer the vertical wavenumber is constant $m_i = \pm N_i/u_0$. Therefore, the influence of partial reflections on surface pressure is described by $\gamma(k) = \gamma_0$ for $k > 0$ and $\gamma(k) = \gamma_0^*$ for $k < 0$ with

$$\gamma_0 = \frac{1 - R \exp(i2H_*)}{1 + R \exp(i2H_*)}. \tag{9}$$

Here, the dimensionless interface height $H_* = HN_1/u_0$ has been introduced. Since γ_0 is independent of k, the surface pressure drag (8) can be written as $D' = (\mathrm{Re}\,\gamma_0) D'_{1L}$, where D'_{1L} denotes the drag in one-layer flow with buoyancy frequency N_1. Evaluating the real part of γ_0 yields

$$D' = \frac{1 - R^2}{1 + 2R\cos(2H_*) + R^2}D'_{1L}. \tag{10}$$

The variation of normalized drag with interface height is independent of the shape of the orography as the gravity waves are nondispersive. Gill's (1982) formula (6.9.10), which was derived for sinusoidal orography, is equivalent to (10). The normalized drag is π-periodic in H_* and varies between $(1 + R)/(1 - R) = N_1/N_2$ and $(1 - R)/(1 + R) = N_2/N_1$. Maximum drag occurs for resonant interface heights: $H_*/\pi = 1, 2, 3, \ldots$ if $N_2 > N_1$, and $H_*/\pi = 1/2, 3/2, 5/2, \ldots$ if $N_2 < N_1$.

To illustrate, we consider a two-layer flow that may represent the troposphere and stratosphere. With typical

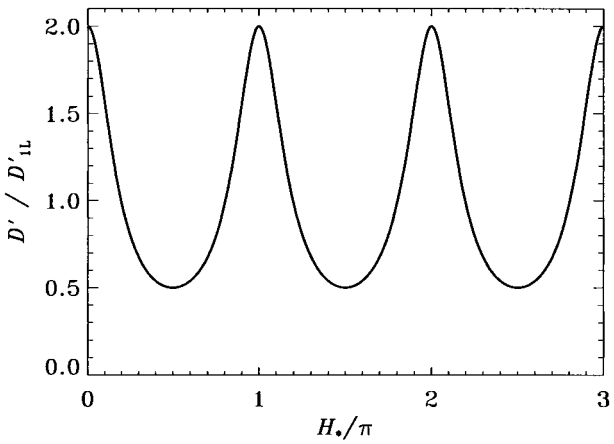

FIG. 2. Variation of normalized drag D'/D'_{1L} with interface height $H_* = HN_1/u_0$ for flow over infinitely long ridges. The reflection coefficient at the interface is $R = -⅓$ corresponding to a ratio of buoyancy frequencies of $N_2/N_1 = 2$.

values of the buoyancy frequency $N_1 = 0.01\ s^{-1}$ and $N_2 = 0.02\ s^{-1}$, the reflection coefficient is $R = -⅓$ at the tropopause. The normalized drag is plotted as a function of interface height for this reflection coefficient in Fig. 2. The range of interface height H_* from 0.5π to 1.5π corresponds to that shown in Fig. 8a in Durran (1992). Note, that the minima are broad in comparison to the pronounced maxima. The dimensionless interface height H_* ranges from 0.8π to 3.2π, if tropopause height and wind speed vary from 6 to 10 km and from 10 to 25 m s^{-1}, respectively. This range of dimensionless interface height covers three maxima and two minima of the normalized drag. Thus, a gradually changing atmospheric flow is likely to experience the entire range of the normalized drag, which is 0.5–2.0 in this example.

4. Drag of axisymmetric mountains

Since gravity waves are dispersive in three-dimensional flow, an analytic result valid for arbitrary orography is not available. However, as will be shown below, it is sufficient to assume an axisymmetric mountain to get an explicit expression for the normalized drag. Let $h(x, y) = h(r)$ denote the orography, where $r = (x^2 + y^2)^{1/2}$. The two-dimensional Fourier transform is then axisymmetric as well $\hat{h}(k, l) = \hat{h}(K)$.

When (6a) is inserted into (7) and (k, l) transformed into polar coordinates (K, ψ), the drag of an axisymmetric mountain becomes

$$D = \frac{\rho_{00} N_1 u_0}{(2\pi)^2} \int_0^{2\pi} \int_0^{\infty} \cos^2(\psi)\gamma(\psi)|\hat{h}(K)|^2 K^2\, dK\, d\psi. \tag{11}$$

With the dispersion relation (5), the factor γ can be written as

$$\gamma(\psi) = \frac{1 - R\ \exp(i2H_*/\cos\psi)}{1 + R\ \exp(i2H_*/\cos\psi)}; \tag{12}$$

that is, it is independent of the magnitude of the wavenumber. Therefore, the integral in (11) can be factorized into two one-dimensional integrals

$$D = I \times D_{1L}, \quad \text{where} \tag{13a}$$

$$I = \frac{1}{\pi} \int_0^{2\pi} \gamma(\psi) \cos^2(\psi)\, d\psi \quad \text{and} \tag{13b}$$

$$D_{1L} = \frac{\rho_{00} N_1 u_0}{4\pi} \int_0^{\infty} |\hat{h}(K)|^2 K^2\, dK. \tag{13c}$$

If both layers have the same buoyancy frequency, there is no reflection: $R = 0$. This yields $\gamma = 1$ and $I = 1$. Therefore, the drag for one-layer flow over an axisymmetric mountain is given by D_{1L}. Equation (13c) proves to be identical to Phillips' (1984) formulas (6.3–6.5) for elliptical mountains in the limit of vanishing eccentricity. Flow over the particular mountain

$$h(r) = h_0(1 + r^2/a^2)^{-3/2} \quad \text{with}$$

$$\hat{h}(K) = 2\pi a^2 h_0 \exp[-aK] \tag{14}$$

is investigated in section 5. This mountain has been used for various analytical studies due to its simple functional form of the Fourier transform (e.g., Smith 1980). The drag of this mountain in a one-layer atmosphere turns out to be

$$D_{1L} = \frac{\pi}{4} \rho_{00} N_1 u_0 h_0^2 a. \tag{15}$$

According to (13a) the normalized drag for two-layer flow is given by the integral I. As shown in the appendix, the integral I can be expanded as a power series in the reflection coefficient

$$I = 1 + 2 \sum_{j=1}^{\infty} (-R)^j F(2jH_*), \tag{16}$$

where the function F is a third integral of the zero-order Bessel function J_0: $F'''(x) = 2J_0(x)$. The constants of integration are $F(0) = 1$, $F'(0) = 0$, and $F''(0) = -2$. The power series can be interpreted as summation over the contribution of gravity waves, that have been reflected once, twice, . . . , j times at the interface. After j reflections, the initial amplitude is reduced by the factor $|R|^j$ and the phase is shifted by $\arccos[(-1)^j] + 2jH_*/\cos\psi$.

The series (16) can be well approximated by simpler formulas. Details are given in the appendix. For a low interface, the series representation of the Bessel function can be used to write I as power series in H_* [Eq. (A5)]. If, on the other hand, the interface is sufficiently high, an asymptotic expression for F can be obtained from the asymptotic behavior of the Bessel function for large arguments [Eq. (A11)]. A low-order truncation of the power series in R is sufficiently accurate unless $|R|$ is very close to 1.

To illustrate, we resume the troposphere/stratosphere

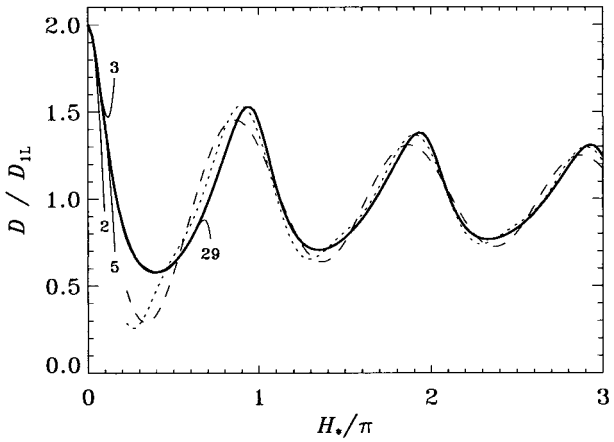

FIG. 3. Variation of normalized drag D/D_{1L} with interface height H_* for flow over axisymmetric mountains. The reflection coefficient is set to $R = -⅓$. The bold curve is calculated by numerical integration of (A1). The other curves represent the analytical approximations derived in the appendix. For low interface, polynomials in H_* of degree $n = 2, 3, 5$ are used, where n is plotted at the end of each curve (solid). For intermediate interface height ($H_* > 0.3$) a polynomial of degree $n = 29$ is used that accounts for three reflections. For high interface, the asymptotic formula for F is employed and the series in R is truncated. The dashed curve accounts for one reflection, the dotted curve for two reflections.

TABLE 1. Overview of finite-amplitude experiments. Dimensionless mountain height $h_* = h_0N_1/u_0$ and interface height $H_* = HN_1/u_0$. Normalized nonlinear surface pressure drag D_{50}/D_{1L} at time $t_* = tu_0/a = 50$, corresponding value D/D_{1L} for linear hydrostatic steady flow given by Eqs. (13a) and (13b). Drag D_{1L} used for the normalization; it is the value given by Eq. (15) for linear hydrostatic steady flow in a one-layer atmosphere with buoyancy frequency N_1.

Expt	h_*	H_*/π	D_{50}/D_{1L}	D/D_{1L}	D_{1L} (10^9 N)
O	0.025	0	1.844*	2.000	0.005709
T1	0.05	0.9	1.382	1.501	0.02092
T2	0.05	1.0	1.513	1.441	0.02032
T3	0.05	1.1	1.360	1.071	0.01973
T4	0.05	1.2	1.072	0.810	0.01914
T5	0.05	1.3	0.870	0.715	0.01855
T6	0.05	1.4	0.792	0.717	0.01796
T7	0.05	1.5	0.784	0.778	0.01739
T8	0.5	0.9	1.332	1.501	2.092
T9	0.5	1.0	1.546	1.441	2.032
T10	0.5	1.1	1.523	1.071	1.973
T11	0.5	1.2	1.248	0.810	1.914
T12	0.5	1.3	0.990	0.715	1.855
T13	0.5	1.4	0.874	0.717	1.796
T14	0.5	1.5	0.841	0.778	1.739
T15**	1.0	1.0	1.500	1.441	8.128
T16	1.0	1.5	0.850	0.778	6.955

* Value increases to 1.858 at $t_* = 100$.
** Flow does not approach a steady state due to wave breaking.

example of the previous section. The normalized drag of axisymmetric mountains is considered for the same reflection coefficient $R = -⅓$, which results from assuming a ratio of buoyancy frequencies of $N_2/N_1 = 2$. The drag is plotted versus interface height in Fig. 3. Besides the analytical formulas, a numerical solution has been calculated. It illustrates the usefulness of the analytical approximations.

As expected due to the 3D dispersion of gravity waves, the variation of drag with interface height is smaller for axisymmetric mountains than for infinitely long ridges. The amplitude of the oscillation of drag reduces asymptotically as $H_*^{-1/2}$ with increasing interface height. The amplitude is decreasing because the spread of the phase of the reflected waves increases with interface height. At the surface, the difference between the phases of two waves reflected j times is equal to $2jH\Delta m$, where Δm denotes the difference between their vertical wavenumbers. Compared to the result for flow over infinitely long ridges, the maxima and minima are shifted slightly toward lower interface heights, as the vertical wavelength of 2D flow is an upper bound to the wavelengths present in 3D flow over isolated mountains.

5. Finite-amplitude experiments

Now we turn to the question of how the drag varies with interface height for flow over finite-height axisymmetric mountains. The troposphere/stratosphere example with $N_2/N_1 = 2$ is continued. A series of 17 numerical simulations with different mountain and tropopause heights is discussed (Table 1).

First, the design of the numerical experiments is described. Then, the drag evolution is analyzed. Finally, the drag in the finite-amplitude experiments is compared with the corresponding values for linear steady flow.

a. Experiment design

The flow over finite-height mountains is numerically simulated with the nonhydrostatic version of the Penn State–NCAR mesoscale model MM5 (Grell et al. 1994; Dudhia 1993). It solves a finite-difference approximation of the compressible equations of motion. The specific setup employed here is described.

Inviscid adiabatic flow of dry air is simulated apart from the mixing by subgrid-scale fluxes and numerical diffusion. As in the previous sections, planetary rotation is not considered. A free-slip condition is employed at the lower boundary. A Rayleigh-damping layer of thickness $D = 2\pi u_0/N_2 = 6.3$ km is implemented at the upper boundary to absorb vertically propagating waves. The flow is relaxed toward the upstream conditions in the absorbing layer. The relaxation rate increases gradually with altitude as $N_2 \cos^2[\pi(z - z_t)/(2D)]$ in the absorbing layer, where z_t is the altitude of the model top. The depth of the absorbing layer and its gradually increasing relaxation rate guarantee that the reflection of vertically propagating gravity waves from the model top is small (Klemp and Lilly 1978).

The 93 model levels are equally spaced with $\Delta z = [(\pi/8)u_0]/N_2 = 393$ m over flat terrain. The model top

is at $z_t = 11.5\pi u_0/N_2 = 36$ km. The domain encompasses an area of 360 km $\times$ 360 km in the horizontal. A grid spacing of 3.6 km is employed. The grid is refined to a spacing of 1.2 km on a subdomain of 120 km $\times$ 120 km. The fine mesh interacts with the coarse mesh. The isolated mountain is located in the center of the subdomain, which is itself centered in the total domain. Large orographically induced perturbations do not reach the lateral boundaries as they are sufficiently distant from the mountain. Additionally, the diffusion on the coarse grid is quite large and damps the gravity waves leaving the subdomain. The drag is calculated on the subdomain, where the gravity waves forced by the mountain are well resolved.

The flow upstream of the mountain is characterized by a wind speed of 20 m s^{-1}, and by buoyancy frequencies of 0.01 s^{-1} and 0.02 s^{-1} in the lower and upper layer, respectively. The tropopause height is varied from 5.6 to 9.4 km corresponding to a dimensionless interface height H_* between 0.9π and 1.5π (experiments T1–T16, Table 1). This range covers part of the variation of H_* expected to occur in the real atmosphere. Additionally one stratosphere-only experiment is performed (experiment O). Profiles of pressure and temperature are obtained from hydrostatic balance. Surface values of pressure and temperature are calculated as a function of tropopause height in such a way that in all experiments an isothermal stratosphere is obtained, in which the pressure decreases with altitude as $p_0(z) = \tilde{p}_{00} \exp(-z/H_s)$. Here H_s denotes the scale height of the isothermal stratosphere. The pressure $\tilde{p}_{00}$ is set to 1138 hPa in all experiments except the stratosphere-only experiment, where 1000 hPa is used. The upstream conditions are modified according to the underlying terrain to obtain the initial conditions. Isentropes are initialized parallel to the terrain-following coordinate surfaces. The velocity field is initialized with a nondivergent flow along the coordinate surfaces.

An axisymmetric mountain given by (14) is used with the width parameter set to $a = 10$ km. As the mountain is broad $aN_1/u_0 = 5 \gg 1$, nonhydrostatic effects are expected to be small. The aim is to study the linear regime and the nonlinear regime of nonbreaking gravity waves. Therefore the dimensionless mountain height $h_* = h_0 N_1/u_0$ is varied from 0.025 to 1.0 (Table 1). In this regime, the entire air stream still passes over the mountain, and the horizontal deflection of the flow remains small.

The mountain given by (14) extends to infinity. Therefore the drag in the area of the subdomain is only a part of the total drag. But it is a large fraction of the total drag as the mountain is lower than $0.004h_0$ outside of the subdomain, which has a size of $12a \times 12a$. The fraction of the drag missed by limiting the calculation to the subdomain is estimated to be around 0.2%. The estimate stems from a numerical solution for linear steady flow in a one-layer atmosphere on a periodic domain of size $102a \times 102a$.

The normalized drag D/D_{1L} of linear steady flow and the corresponding values for a one-layer atmosphere D_{1L} given by equations (13a), (13b), and (15) are listed in Table 1 for the parameter settings of the finite-amplitude experiments. For a given mountain height h_0, the one-layer drag D_{1L} is not constant. This results from the choice of the upstream conditions. The drag D_{1L} depends on the surface density ρ_{00}, which is a function of tropopause height.

b. Drag evolution

The flow approaches a steady state in all experiments except T15. This particular experiment is the only one in which wave breaking occurs. The wave breaking is seen as the cause of the unsteadiness of the flow. Figure 4 shows the temporal evolution for the experiments with tropopause height $H_* = 1.0\pi$ and 1.5π. In experiment T15 the normalized drag varies between 1.0 and 1.8 after $t_* = 10$. Here, the dimensionless time $t_* = tu_0/a$ is defined via the advective timescale. The drag is almost constant after $t_* = 10$ in all other experiments.

The surface pressure can be affected by the presence of the tropopause after the time required for the orographic gravity waves to propagate from the surface to the tropopause and back. For a linear hydrostatic steady gravity wave with wavenumber (k, l), this time is given by

$$t_p = \frac{2H}{c_{gz}} \quad \text{with } c_{gz} = \frac{u_0^2 k^2}{N_1 (k^2 + l^2)^{1/2}}, \tag{17}$$

where c_{gz} denotes the vertical component of the group velocity in the troposphere. Waves with the typical wavenumber $(k, l) = (a^{-1}, 0)$ require a time of

$$t_{p*} = t_p u_0/a = 2H_* \tag{18}$$

to propagate from the surface to the tropopause and back again. For the range of tropopause height investigated here, t_{p*} lies between 6 and 9. The estimated timescale t_{p*} is consistent with the evolution of the drag in the finite-amplitude experiments without wave breaking, as the drag changes little after $t_* = 10$.

The arrival of waves reflected several ($n \geq 2$) times at the interface requires a time of $nt_{p*} \geq 12$ for waves with the typical wavenumber $(k, l) = (a^{-1}, 0)$. The small change of drag occurring after $t_* = 10$ in the numerical experiments suggests that multiple reflections only lead to a minor change of the drag. A small contribution of multiple reflections is expected from the analytical results, as the single reflection term in (16) is the leading order correction that accounts for the two-layer structure of the flow.

c. Linear versus finite-amplitude drag

Now we compare the drag of the finite-amplitude experiments at $t_* = 50$ with the drag of linear steady flow. All experiments (except T15) have evolved into an al-

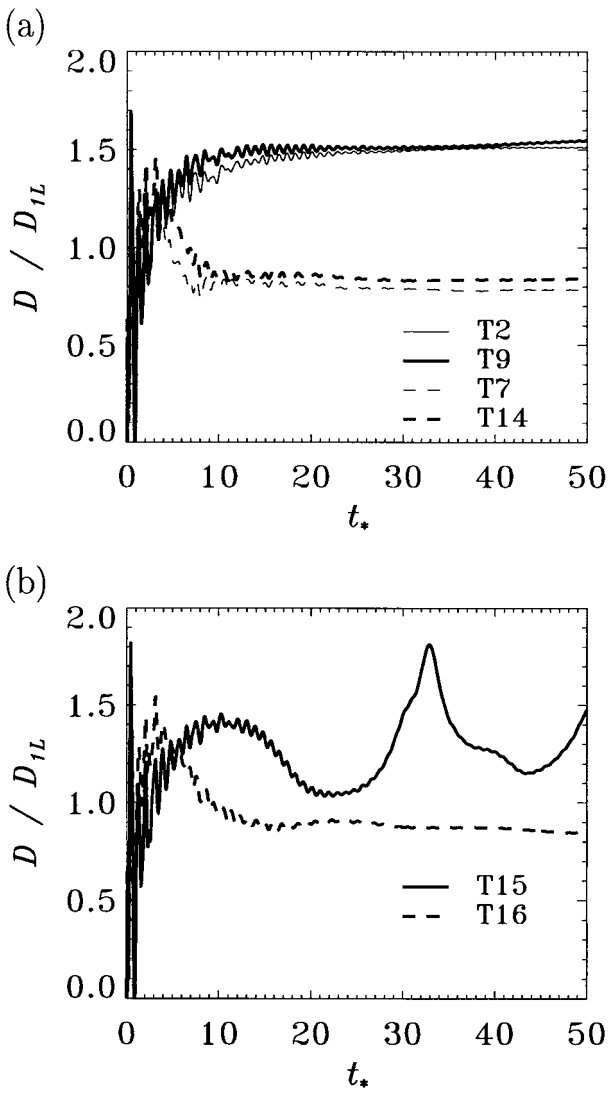

FIG. 4. Evolution of normalized drag in the finite-amplitude experiments with dimensionless interface height 1.0π (solid) and 1.5π (dashed). (a) Mountain height $h_* = 0.05$ (thin) and $h_* = 0.5$ (heavy) (experiments T2, T7, T9, and T14); (b) mountain height $h_* = 1$ (experiments T15 and T16). The dimensionless time is defined as $t_* = tu_0/a$.

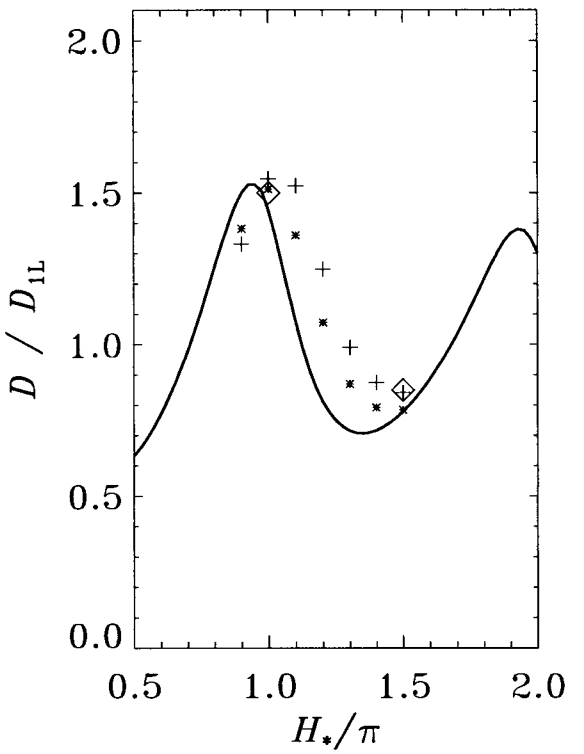

FIG. 5. Finite-amplitude effects on the variation of normalized drag with interface height for axisymmetric mountains. The curve represents the normalized drag calculated from linear theory of steady hydrostatic flow, and the symbols mark the value of the nonlinear numerical experiments at dimensionless time $t_* = 50$. The different symbols code the dimensionless mountain height: $h_* = 0.05$ (asterisk), 0.5 (plus signs), and 1 (diamonds).

most steady state at this time. The wave amplitude is not the only difference between linear theory and finite-amplitude experiments. Additionally, the following differences can affect the drag: (i) steady flow/initial value problem, (ii) drag calculated on infinite/finite domain, (iii) hydrostatic/nonhydrostatic dynamics, (iv) analytic solution/finite-difference approximation, and (v) Boussinesq/compressible flow. None of the points (i)–(v) is expected to cause large differences of the drag. The combined effect of (i)–(v) is seen in the experiments T1–T7, and O because the mountain is low and nonlinear effects are small in these experiments (Table 1). The normalized drag in the one-layer experiment O attains 92% of the value predicted by linear theory at $t_* = 50$. In the subset of low mountain experiments, T4 deviates most from the linear theory prediction. The normalized drag is 32% larger at $t_* = 50$ than the corresponding value from linear theory.

The normalized drag at $t_* = 50$ is plotted versus interface height for all two-layer experiments in Fig. 5. The variation of the drag in the linear regime, mountain height $h_* = 0.05$, is similar to the prediction of linear theory. The same values as in linear theory are attained at a higher interface. The shift of interface height H_* is approximately 0.25.

The experiments with mountain height $h_* = 0.5$ exhibit a small additional shift toward higher interface of $\Delta H_* \approx 0.15$ as compared to the experiments with $h_* = 0.05$. Furthermore, the maximum at $H_* = 1$ is slightly narrower for the low mountain.

The change in interface height from 1.5π to 1.0π causes a transition to the regime of breaking gravity waves at a mountain height $h_* = 1.0$. The drag in experiment T15 remains unsteady throughout the integration (Fig. 4b). Therefore the value at $t_* = 50$ is not representative and it is a coincidence that it is close to the prediction of linear theory.

6. Discussion

This work has focused on the variation of drag with interface height for steady hydrostatic two-layer flow over infinitely long ridges and mountains with circular contours. The partial reflection of gravity waves at the interface results in a drag that varies with interface height in an oscillatory manner. In 3D flow, the amplitude of the oscillation of drag with interface height is smaller than in 2D flow. The different spectra of vertical wavelength cause the different behavior. In 2D flow, all gravity wave energy is concentrated at the single vertical wavenumber N/u_0, whereas in 3D flow over isolated mountains the wave energy is distributed with N/u_0 being the smallest vertical wavenumber excited.

Finite-amplitude experiments for two-layer flow over isolated mountains were performed to determine to what extent the linear theory predictions describe the drag of nonlinear flow. The experiments represent a troposphere–stratosphere flow, that is, higher stability in the upper layer. The variation of nonlinear drag obtained from the experiments that evolve into a steady state is very similar to the variation of linear drag. The amplitudes of nonlinear variations and linear variations are almost equal. The main finite-amplitude effect is that the drag versus interface height relation is shifted toward higher interface. The shift in interface height H_* determined from the experiments with mountain height $h_* = 0.5$ is $\Delta H_* \approx 0.4 = 0.8h_*$ if compared to linear theory and $\Delta H_* \approx 0.15 = 0.3h_*$ if compared to the low mountain experiments. In two-dimensional flow the finite-amplitude effect is larger. Durran (1992) determined a shift of $\Delta H_* \approx 1.5h_*$ for mountain height $h_* \leq 0.5$. Thus, linear theory better approximates the finite-amplitude drag for flow over isolated mountains than for flow over infinitely long ridges.

It would be interesting to extend the investigation to isolated mountains with elliptical contours, such as the family of mountains studied by Phillips (1984). The spectrum of vertical wavenumber of an elliptical mountain oriented normal to the flow is more focused at N/u_0 than that of a corresponding circular mountain. Therefore, elliptical mountains oriented normal to the flow are expected to exhibit a larger variation of normalized drag with interface height than circular mountains and a smaller variation than infinitely long ridges. By the same sort of argument, elliptical mountains oriented along-flow will exhibit a smaller variation of normalized drag with interface height than circular mountains.

Here, partial reflection was examined for a discontinuous change of buoyancy frequency at the interface between two layers. Continuous changes of buoyancy frequency in a layer of a certain depth are a more realistic description of the atmosphere. Such continuous changes are less reflective than the discontinuous change. Blumen's (1985) analysis of continuous reflection in 2D flow shows that the reflection coefficient is reduced by a factor of 0.85 when the buoyancy frequency changes over a vertical scale of $\frac{1}{3}u_0(N_1 + N_2)^{-1}$. This scale is of the order of 0.3 km for typical atmospheric values. A more gradual change further reduces the reflection coefficient. In 3D flow, the reflectivity of a layer with a continuous change of buoyancy frequency will depend on the vertical wavenumber, that is, on the orientation of the horizontal wavenumber vector via the dispersion relation. A change of buoyancy frequency over a certain vertical scale appears more gradual for a wave with smaller vertical wavelength than for a wave of larger vertical wavelength.

The analytical expressions for the normalized drag have been illustrated with a troposphere–stratosphere type of flow with a reflection coefficient of $|R| = ⅓$ at the tropopause. This is a rather moderate reflection; real atmospheric profiles can be more reflective for hydrostatic gravity waves. Blumen and Hartsough (1985) present reflection coefficients calculated from radiosonde data. For flow past the Pyrénées on 23 March 1982 the magnitude of the reflection coefficient reaches 0.5, and during the 11 January 1972 Boulder wind storm the magnitude of the reflection coefficient exceeds 0.8.

Results from general circulation models and global numerical weather prediction models improved as parameterizations of the orographic gravity wave drag (GWD) were introduced (Palmer et al. 1986; McFarlane 1987). Most current GWD schemes estimate the low-level momentum flux solely from near-surface values of wind speed, direction, and buoyancy frequency. To obtain the vertical structure of the wave and the associated stress, a saturation hypothesis and the WKBJ approximation are employed. By making the WKBJ approximation internal reflections of gravity waves are neglected. Laprise (1993) compares the momentum fluxes obtained from the WKBJ method and those from a column model of the linearized dynamics, which accounts for the internal reflection of gravity waves. Profiles of wind speed and buoyancy frequency at a midlatitude location were taken from a GCM integration over one winter month. On specific dates the WKBJ estimate of the surface pressure drag is larger or smaller than the value of the column model by a factor as large as 2. But the time average value of the surface pressure drag in the WKBJ method is quite close to the corresponding average value of the column model. Thus, it is expected that the neglect of internal reflections does not introduce a bias of the time mean drag, if the timescale is sufficiently long. However, in weather forecasting the desired result is the state of the atmosphere at a specific time. A GWD scheme that generates the correct time mean drag may still be detrimental for a forecast. Hence, there may be a potential for improvements if the enhancement and reduction of the surface pressure drag caused by internal reflections could be incorporated into a GWD scheme. Gregory et al. (1998) attempt to account for the effect of partial reflections by using a variable depth two-dimensional two-layer model to estimate the *reduction* of the drag due to partial

reflections. However, the *amplification* of the drag is disregarded.

This paper investigated the modification of surface pressure drag caused by partial reflections of gravity waves in two-layer flow over axisymmetric mountains. It is one step within the general effort to improve our understanding of the momentum redistribution due to orographic gravity waves.

Acknowledgments. Comments by Andreas Dörnbrack and Hans Volkert on an earlier version of the manuscript helped improving the presentation of the material. Three anonymous reviewers provided further constructive suggestions. This work is part of the author's doctoral thesis at the University of Munich. The Institut für Physik der Atmosphäre, Deutsches Zentrum für Luft- und Raumfahrt, Oberpfaffenhofen, Germany, provided the funding and a favorable research environment.

APPENDIX

Evaluation of Integral I

As a first step to evaluate the integral I analytically, it is convenient to rewrite (13b) as

$$I = \frac{4}{\pi}\mathrm{Re}\int_0^{\pi/2} \gamma(\psi)\cos^2(\psi)\,d\psi \tag{A1}$$

by splitting the interval $[0, 2\pi]$ into four equal parts and employing $\gamma(\psi + \pi) = \gamma^*(\psi)$.

a. Series expansion in R

The power series (16) is obtained from (A1) by using a geometric series in $\zeta = -R\exp(i2H_*/\cos\psi)$. We express

$$\gamma = \frac{1+\zeta}{1-\zeta} = (1+\zeta)\sum_{j=0}^{\infty}\zeta^j = 1 + 2\sum_{j=1}^{\infty}\zeta^j \tag{A2a}$$

to get

$$\mathrm{Re}\gamma = 1 + 2\sum_{j=1}^{\infty}(-R)^j\cos(2H_* j/\cos\psi). \tag{A2b}$$

By inserting (A2b) in (A1) and interchanging integration and summation, we get the power series (16), where the function F is defined as

$$F(x) = \frac{4}{\pi}\int_0^{\pi/2}\cos(x/\cos\psi)\cos^2\psi\,d\psi. \tag{A3a}$$

Transformation to the variable $t = 1/\cos\psi$ yields

$$F(x) = \frac{4}{\pi}\int_1^{\infty}\frac{\cos(xt)}{t^3\sqrt{t^2-1}}\,dt. \tag{A3b}$$

The function F is intimately related to the zero-order Bessel function J_0, which can be expressed as $J_0(x) = (2/\pi)\int_1^{\infty}(t^2-1)^{-1/2}\sin(xt)\,dt$ (Gradshteyn and Ryzhik 1994). As a consequence, $F'''(x) = 2J_0(x)$. This relation and the three constants of integration $F(0) = 1$, $F'(0) = 0$, $F''(0) = -2$ completely determine the function F. The relation between F and J_0 will be exploited in the following approximations.

b. Approximation for small and intermediate interface height

To derive an approximation for a ''low'' interface, I is expanded into a power series in H_*. First, F is calculated by integrating the series expansion of the Bessel function

$$F(x) = 1 - x^2 + 2\sum_{k=0}^{\infty}\frac{(-1)^k x^{2k+3}}{2^{2k}(2k+1)(2k+2)(2k+3)(k!)^2}. \tag{A4}$$

Employing this relation in (16) and changing the order of summation results in the desired power series in H_*:

$$I = 1 + 2\sigma_0(-R) - 8\sigma_2(-R)H_*^2 + \sum_{k=0}^{\infty}\frac{32(-1)^k\sigma_{2k+3}(-R)}{(2k+1)(2k+2)(2k+3)(k!)^2}H_*^{2k+3}, \tag{A5}$$

where

$$\sigma_\nu(q) = \sum_{j=1}^{\infty} j^\nu q^j = \left(q\frac{d}{dq}\right)^\nu\sigma_0(q) \tag{A6}$$

and $\sigma_0(q) = q/(1-q)$. For a ''low'' interface the series (A5) can be truncated to a polynomial in H_* without changing the result much.

For intermediate interface heights, the convergence of the polynomials to the integral I is considerably improved if only a finite number N of reflections is taken into account. This is equivalent to replacing σ_ν in (A5) by $\sigma_\nu^{(N)}$, where

$$\sigma_\nu^{(N)}(q) = \sum_{j=1}^{N} j^\nu q^j. \tag{A7}$$

c. Approximation for high interface

A useful approximation of (16) for a ''high'' interface involves an asymptotic formula for $F(x)$ valid for large x. Additionally, the power series in R can be truncated after the first few terms. Let a specific third integral of the Bessel function J_0 be defined as

$$G(x) = -\int_x^{\infty}\left[\int_{x'}^{\infty}\left(\int_y^{\infty}J_0(z)\,dz\right)dy\right]dx'. \tag{A8}$$

For the approximation, we make use of the asymptotic behavior of the Bessel function for large argument x (Gradshteyn and Ryzhik 1994):

$$J_0(x) = \left[\frac{2}{(\pi x)}\right]^{1/2}\left\{\sin\left(x + \frac{\pi}{4}\right)[1 + O(x^{-2})] + \cos\left(x + \frac{\pi}{4}\right)O(x^{-1})\right\}, \quad \text{(A9)}$$

where $O(x^{-n})$ denotes a term of the order of x^{-n}. After inserting (A9) into (A8), it can be shown by partial integrations that

$$G(x) = \left[\frac{2}{(\pi x)}\right]^{1/2}\cos\left(x + \frac{\pi}{4}\right) + O(x^{-3/2}). \quad \text{(A10)}$$

The function G is the unique third integral of J_0 with $\lim_{x\to\infty} G(x) = 0$. As $\frac{1}{2}F$ is a third integral of J_0 with $\lim_{x\to\infty} F(x) = 0$, it follows that $F = 2G$. Therefore, F can be approximated by

$$F(x) = \left[\frac{8}{(\pi x)}\right]^{1/2}\cos\left(x + \frac{\pi}{4}\right) \quad \text{(A11)}$$

with an error of $O(x^{-3/2})$.

REFERENCES

Bacmeister, J. T., and R. T. Pierrehumbert, 1988: On high-drag states of nonlinear stratified flow over an obstacle. *J. Atmos. Sci.,* **45,** 63–80.

——, and M. R. Schoeberl, 1989: Breakdown of vertically propagating two-dimensional gravity waves forced by orography. *J. Atmos. Sci.,* **46,** 2109–2134.

Blumen, W., 1965: A random model of momentum flux by mountain waves. *Geofys. Publ.,* **26,** 1–33.

——, 1985: Reflection of hydrostatic gravity waves in a stratified shear flow. Part I: Theory. *J. Atmos. Sci.,* **42,** 2255–2263.

——, and C. S. Hartsough, 1985: Reflection of hydrostatic gravity waves in a stratified shear flow. Part II: Application to downslope surface windstorms. *J. Atmos. Sci.,* **42,** 2320–2331.

Clark, T. L., and W. R. Peltier, 1977: On the evolution and stability of finite-amplitude mountain waves. *J. Atmos. Sci.,* **34,** 1715–1730.

Dudhia, J., 1993: A nonhydrostatic version of the Penn State–NCAR mesoscale model: Validation tests and simulation of an Atlantic cyclone and cold front. *Mon. Wea. Rev.,* **121,** 1493–1513.

Durran, D. R., 1986: Another look at downslope wind storms. Part I: The development of analogs to supercritical flow in an infinitely deep continously stratified fluid. *J. Atmos. Sci.,* **43,** 2527–2543.

——, 1992: Two-layer solutions to Long's equation for vertically propagating mountain waves: How good is linear theory? *Quart. J. Roy. Meteor. Soc.,* **118,** 415–433.

——, and J. B. Klemp, 1987: Another look at downslope winds. Part II: Nonlinear amplification beneath wave-overturning layers. *J. Atmos. Sci.,* **44,** 3402–3412.

Eliassen, A., and E. Palm, 1960: On the transfer of energy in stationary mountain waves. *Geofys. Publ.,* **22,** 1–23.

Gill, A. E., 1982: *Atmosphere–Ocean Dynamics.* Academic Press, 662 pp.

Gradshteyn, I. S., and I. M. Ryzhik, 1994: *Table of Integrals, Series, and Products.* 5th ed. Academic Press, 1204 pp.

Gregory, D., G. J. Shutts, and J. R. Mitchell, 1998: A new gravity-wave-drag scheme incorporating anisotropic orography and low-level wave breaking: Impact upon the climate of the UK Meteorological Office Unified Model. *Quart. J. Roy. Meteor. Soc.,* **124,** 463–493.

Grell, G. A., J. Dudhia, and D. R. Stauffer, 1994: A description of the fifth-generation Penn State/NCAR mesoscale model (MM5). NCAR Tech. Note NCAR/TN-398 + IA, 120 pp.

Grubišić, V., and P. Smolarkiewicz, 1997: The effect of critical levels on 3D orographic flows: Linear regime. *J. Atmos. Sci.,* **54,** 1943–1960.

Klemp, J. B., and D. K. Lilly, 1975: The dynamics of wave-induced downslope winds. *J. Atmos. Sci.,* **32,** 320–339.

——, and ——, 1978: Numerical simulation of hydrostatic mountain waves. *J. Atmos. Sci.,* **35,** 78–109.

Laprise, J. P. R., 1993: An assessment of the WKBJ approximation to the vertical structure of linear mountain waves: Implications for gravity-wave drag parameterization. *J. Atmos. Sci.,* **50,** 1469–1487.

Lilly, D. K., and J. B. Klemp, 1979: The effects of terrain shape on nonlinear hydrostatic mountain waves. *J. Fluid Mech.,* **95,** 241–251.

McFarlane, N. A., 1987: The effect of orographically excited gravity wave drag on the general circulation of the lower stratosphere and troposphere. *J. Atmos. Sci.,* **44,** 1775–1800.

Miranda, P. M. A., and I. N. James, 1992: Non-linear three-dimensional effects on gravity wave drag: Splitting flow and breaking waves. *Quart. J. Roy. Meteor. Soc.,* **118,** 1057–1081.

Ólafsson, H., and P. Bougeault, 1997: The effect of rotation and surface friction on orographic drag. *J. Atmos. Sci.,* **54,** 193–210.

Palmer, T. N., G. J. Shutts, and R. Swinbank, 1986: Alleviation of a systematic westerly bias in general circulation and numerical weather prediction models through an orographic gravity wave drag parameterization. *Quart. J. Roy. Meteor. Soc.,* **112,** 1001–1039.

Phillips, D. S., 1984: Analytical surface pressure and drag for linear hydrostatic flow over three-dimensional elliptical mountains. *J. Atmos. Sci.,* **41,** 1073–1084.

Queney, P., 1947: Theory of perturbations in stratified currents with applications to airflow over mountain barriers. Misc. Rep. 23, Department of Meteorology, University of Chicago, Illinois, 81 pp. [Available from The University of Chicago Press, 5801 Ellis, Chicago, IL 60637.]

——, 1948: The problem of air flow over mountains: A summary of theoretical studies. *Bull. Amer. Meteor. Soc.,* **29,** 16–27.

Scorer, R. S., 1949: Theory of lee waves of mountains. *Quart. J. Roy. Meteor. Soc.,* **75,** 41–56.

Smith, R. B., 1977: The steepening of hydrostatic mountain waves. *J. Atmos. Sci.,* **34,** 1634–1654.

——, 1979: The influence of mountains on the atmosphere. *Advances in Geophysics,* Vol. 21, Academic Press, 87–230.

——, 1980: Linear theory of stratified hydrostatic flow past an isolated mountain. *Tellus,* **32,** 348–364.

——, 1989: Hydrostatic airflow over mountains. *Advances in Geophysics,* Vol. 31, Academic Press, 1–41.

Zierep, J., 1956: Das Verhalten der Leewellen in der Stratosphäre. *Beitr. Phys. Atmos.,* **29,** 10–20.